Experimental study on lead extrusion damper and its earthquake mitigation effects for large-span reticulated shell

M.F. Yang [1,2a], Z.D. Xu [*1] and X.C. Zhang [1a]

[1] *Key Laboratory of C&PC Structures of the Ministry of Education,
Southeast University, Nanjing 210096, China*
[2] *School of Civil Engineering and Architecture,
Anhui University of Science and Technology, Huainan 232001, China*

Abstract. A Lead Extrusion Damper (LED) is experimentally studied under various frequencies and displacement amplitudes. Experimental results show that the force-displacement hysteresis loops of the LED are close to rectangular and the force-velocity hysteresis loops exhibit nonlinear hysteretic characteristic. Also, the LED can provide consistent energy dissipation without any stiffness degradation. Based on the experimental results, a mathematical model is then proposed to describe the effects of frequency and displacement on property of LED. It can be proved from the comparison between experimental and numerical results that the mathematical model can accurately describe the mechanical behavior of LED. Subsequently, the seismic responses of the Schwedler reticulated shell structure with LEDs are analyzed by ANSYS software, in which three different installation forms of LEDs are considered. It can be concluded that the LED can effectively reduce the displacement and acceleration responses of this type of structures.

Keywords: large-span reticulated shell; lead extrusion damper (LED); mathematical model; dynamic analysis; vibration control

1. Introduction

In traditional anti-seismic design the anti-seismic performances of a structure is ensured by increasing strength and ductility of their structural members. However, this design method of resisting earthquake is neither economic nor logical. Even though modern structural design methods seek to localize damage to specific areas such as plastic hinge zones, the associated damage can be difficult and expensive to repair (Housner *et al*. 1997, Towashiraporn *et al*. 2002, Garlock *et al*. 2005). So it is possible to resort to the structure energy absorbing devices which absorb most of its energy of motion (Kato *et al*. 2005). Lead Extrusion Damper (LED) is such an energy absorber device which uses lead as the damping material, due to its unique rheological properties and low recrystallisation temperature.

In 1976, the LED has been developed and tested over a wide range of conditions (Robinson and

---

∗Corresponding author, Professor, E-mail: xuzhdgyq@seu.edu.cn
[a] Ph.D., E-mail: yangmf_aust@163.com

Greenbank 1976, Cousins and Porritt 1993). The test results show that the force-displacement hysteresis loop behaves liked "Coulomb damper" at ambient temperatures and that the lead was able to be "hot worked" over many cycles. Subsequently, the velocity-dependent model was proposed to describe the relationship between the extrusion force and the velocity of bulged-shaft. But the temperature effect could not be reflected in this model. Considering this limitation, the mathematical model considering temperature effect was proposed by Tsai *et al*. (2002). However, the extrusion force calculation is too complex and more parameters have to be determined. To simplify the solution to the extrusion force, a more simplified empirical model was proposed by Rodgers *et al*. (2006). During this period, a large number of researches about the vibration control of the structure by using the LED have been carried out (Aida *et al*. 1998, B ley *et al*. 2008, Bel Hadj Ali and Smith 2010). The stresses in the coolant channel due to earthquake were reduced significantly when practical application of the LED was used in India (2004), and response spectrum analysis was also carried out. Response spectrum analysis results and the nonlinear time history analysis results show good agreement. In 2008, a special LED was also experimentally tested and applied to a jointed precast concrete connection in University of Canterbury (Rodgers *et al*. 2008), and the LED developed was smaller and more compact for structural applications like base-isolation. But the LED still provided the same force levels in a significantly smaller package, greatly extending the possible applications. In recent years, the vibration control of reticulated shell structure has become one of the most important topics. The vertical and horizontal shaking table tests on large-span reticulated shell structures with viscoelastic multi-dimensional earthquake isolation and mitigation devices were studied by Xu (2009). In order to design and evaluate the active control devices of bridge, the CFD model was adopted in the analytic process (Manenti *et al*. 2010). But so far, there are few related researches on LED application in reticulated shell structure.

In order to study the performances of LED used in the large-span reticulated shell, a full-scale LED is experimentally studied in this paper. The effects of frequency and displacement amplitude on hysteresis loops of LED are analyzed. Then, a mathematical model based on the experimental results is proposed, and comparisons between experimental and numerical results are carried out. At last, earthquake mitigation effect of large-span reticulated shell structure with LEDs is numerical analyzed by ANSYS software.

2. Experiment and results analysis

2.1 LED description and experimental setup

The schematic diagram of a LED, consisting of steel cylinder, bulged-shaft and pure lead, can be seen in Fig. 1.

The steel cylinder and bulged-shaft are both made of Q235 steel and were worked with great accuracy to ensure the contact surface smoothness in the machining process of the components. Lead with the purity of 99.99% is heated to melt completely, and then poured into the steel cylinder. It must be paid attention to prevent voids in the process of perfusion. The stroke is 50 mm. The other dimensions of the LED are shown in Table 1.

In order to study the mechanical properties, energy dissipation and anti-fatigue properties of the LED, specific performance tests were carried out. The schematic layout and a picture of the experimental setup are shown in Fig. 2. The loading device was an electro-hydraulic fatigue testing machine, whose maximum load and stroke are 1000 kN and 150 mm, respectively. In the
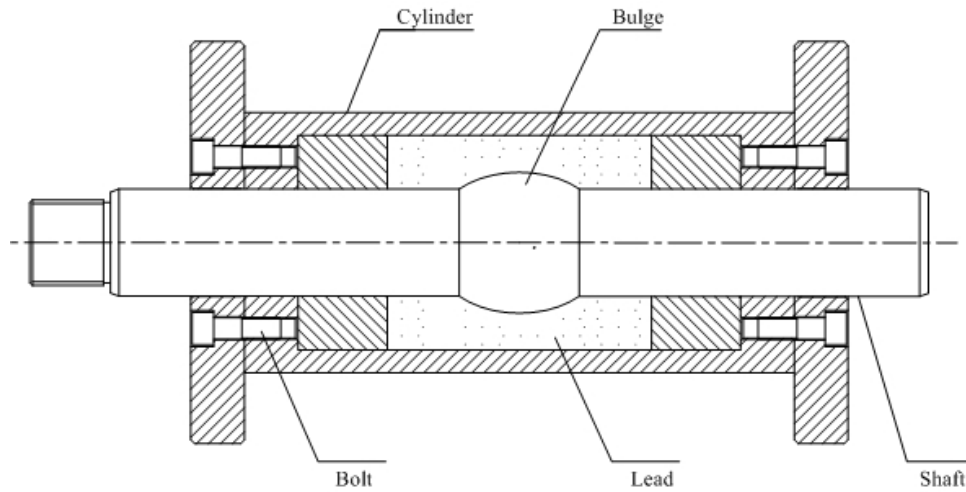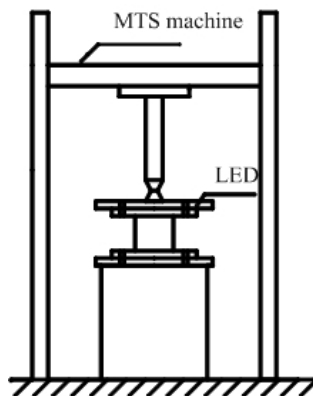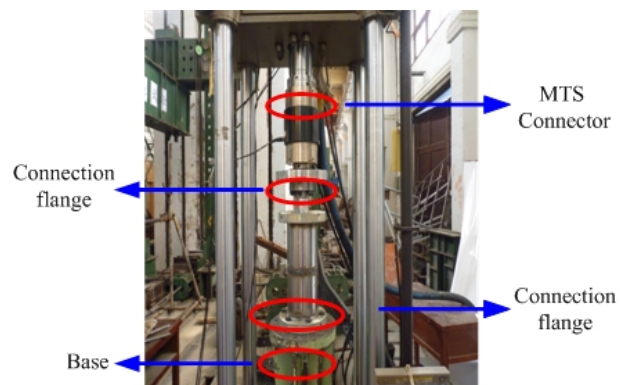
Fig. 1 Schematic diagram of LED

Table 1 Main geometric parameters of LED

Cylinder outer diameter (mm)	194	LED length (mm)	650
Cylinder inner diameter (mm)	160	Bulge height (mm)	7
Guide bar diameter (mm)	80	Bulge length (mm)	70

(a) Experimental design　　　　(b) Physical design

Fig. 2 Test photograph of LED

experiment, the LED was subjected to a sinusoidal displacement excitation. The sinusoidal displacement excitation can be expressed as $u = A\sin(2\pi ft)$, where A is the displacement amplitude, f is the excitation frequency, and t is the loading time. Tests were conducted at selected displacement amplitudes and excitation frequencies. The excitation frequencies are 0.1 Hz, 0.2 Hz, 0.5 Hz, and 0.7 Hz respectively. At each frequency, the displacement amplitudes are 10 mm, 15 mm, 20 mm, and 25 mm, respectively. Each test consists of ten cycles of sinusoidal excitation with

fixed displacement amplitude and frequency. Tests are carried out under the environmental temperature of 25~32°C. In the fatigue tests, the LED was subjected to 500 loading cycles.

2.2 Results analysis

The single hysteresis loop in the stable state is chosen as representative for research in this paper. Typical hysteresis loops of the LED under various frequencies and displacement amplitudes are shown in Figs. 3-4. It can be seen from Figs. 3-4 that the force-displacement hysteresis loops exhibit rectangular shape, and the force-velocity hysteresis loops exhibit nonlinear hysteretic characteristic.
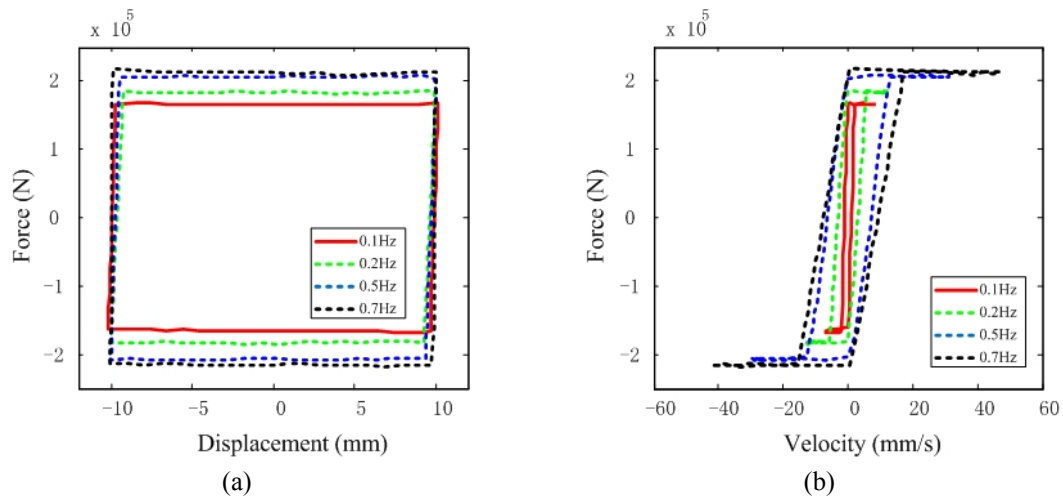

(a)   (b)

Fig. 3 Force-displacement and force-velocity hysteresis loops under 10 mm displacement amplitude and various frequencies

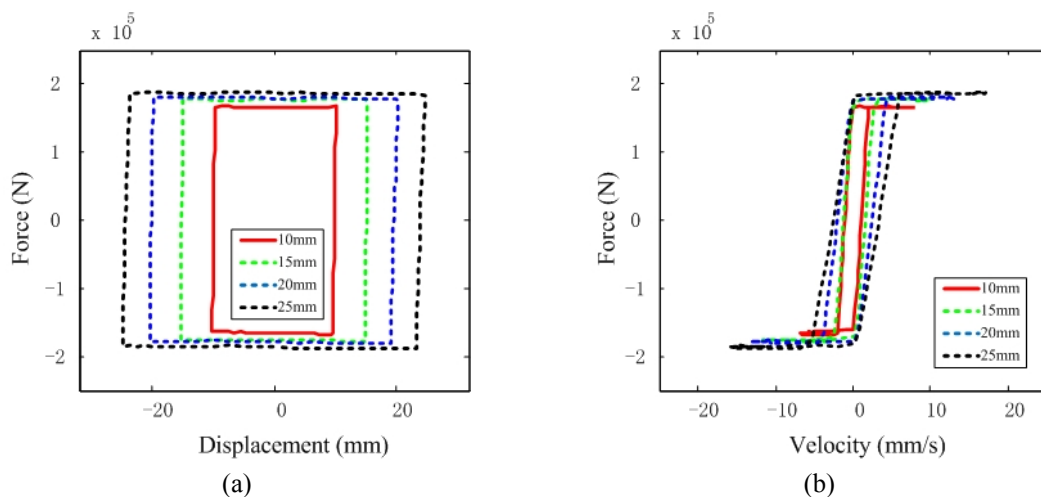(a)   (b)

Fig. 4 Force-displacement and force-velocity hysteresis loops under 0.1 Hz frequency and various displacement amplitudes

Table 2 Maximum extrusion forces of LED under different excitation frequencies

Excitation frequency (Hz)	0.1	0.2	0.5	0.7
Maximum extrusion force (kN)	167.8	185.0	208.2	217.5

Table 3 Maximum extrusion forces of LED under different displacement amplitudes

Displacement amplitude (mm)	10	15	20	25
Maximum extrusion force (kN)	167.8	178.3	182.0	188.9

2.2.1 Excitation frequency effect

Table 2 lists the maximum extrusion forces of LED under different excitation frequencies. From Table 2, the maximum extrusion forces under the excitation frequencies of 0.1 Hz, 0.2 Hz, 0.5 Hz, and 0.7 Hz are 167.8 kN, 185.0 kN, 208.2 kN, and 217.5 kN, respectively, then the corresponding percentage increments of the maximum extrusion force compared to the 0.1 Hz frequency are 10%, 24%, and 30%, respectively. These data demonstrate that the maximum extrusion force of LED increases with increasing frequencies, but the increase rate is gradually slowing. One of the main reasons is because the yield strength of lead is affected by temperature and atomic structure, but the influence is limited (Karolvzuk and Macha 2005, Wu 2008). The results of these effects tend to be stable as the temperature increases. Fig. 3 details the variation of the force-displacement and force-velocity hysteresis loops with frequency, in which the displacement amplitude is 10 mm. From Fig. 3, the force-velocity curves also exhibit a nonlinear hysteretic characteristic. When the velocity amplitude increases, the widths of the force-velocity curves increase significantly. At the same time, the slope of the single force-velocity curve in the low velocity zone decreases slightly with frequency at the displacement amplitude of 10 mm. These mainly caused by an increase in maximum extrusion force.

2.2.2 Displacement amplitude effect

Table 3 lists the maximum extrusion forces of LED under different displacement amplitudes. From Table 3, the maximum extrusion forces under the displacement amplitudes of 10 mm, 15 mm, 20 mm, and 25 mm are 167.8 kN, 178.3 kN, 182.0 kN, and 188.9 kN, respectively. Then the corresponding percentage increments of the maximum extrusion force compared to 10 mm displacement amplitude are 6%, 9%, and 13%, respectively. Fig. 4 shows the variation of the force-displacement and force-velocity hysteresis loop with displacement amplitude, in which the excitation frequency is 0.1 Hz. From Fig. 4, the maximum extrusion force of LED increases slightly with increasing displacement amplitude when excitation frequency is constant. The same as the frequency effect, the slope of the single force-velocity curve in the low velocity zone decreases with displacement amplitude increasing under fixed frequency. This behavior is mainly caused by the increase of displacement amplitude or velocity amplitude.

2.2.3 Energy dissipation

Generally, the energy dissipation value E_d of LED can be obtained by calculating the area enclosed by per cycle of the force-displacement hysteresis curve, E_d is given by

Table 4 Energy dissipation of LED (kJ)

Frequency (Hz)	10	15	20	25
0.1	6.59	10.73	14.35	18.11
0.2	7.07	10.98	15.29	19.49
0.5	8.07	12.45	17.45	21.82
0.7	8.53	13.12	18.35	23.83

$$E_d = \int F(t)\mathrm{d}u = \int_0^{1/f} F(t)\dot{u}\mathrm{d}t \tag{1}$$

where, u and $\dot{u}$ are the piston displacement and the velocity of the damper respectively, and f is the excitation frequency.

The energy dissipations of LED calculated based on experimental results are listed in Table 4. From Table 4, the energy dissipation of the LED increases obviously when the displacement amplitude increases under fixed frequency. Taking 0.1 Hz frequency as an example, the energy dissipation values under the displacement amplitudes of 10 mm, 15 mm, 20 mm, and 25 mm are 6.59 kJ, 10.73 kJ, 14.35 kJ, and 18.11 kJ, respectively. It is clearly observed that the energy dissipation at the displacement amplitude of 25 mm is 2.75 times larger than that of 10 mm displacement amplitude. However, energy consumption has a slight increase with the increase of frequency. In the case of 10 mm displacement amplitude, the energy dissipation at the frequency of 0.7 Hz only increases 29.4% compared with 0.1 Hz frequency, and the increasing rates are only 22.3%, 27.9%, and 31.6%, respectively under the displacement amplitudes of 15 mm, 20 mm, and 25 mm. This means that the frequency has a smaller impact on energy consumption. These phenomena demonstrate that the LED possesses excellent capability of energy dissipation. Also, the energy dissipation increases with the increase of both the frequency and displacement amplitude, in particular, displacement amplitude.
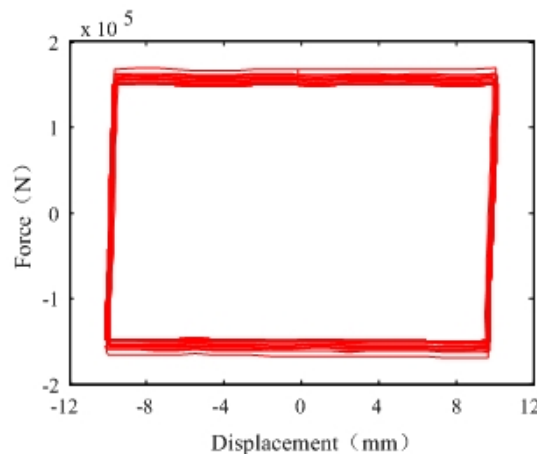

Fig. 5 The fatigue hysteresis loops under 0.1 Hz frequency and 10 mm displacement amplitude

2.2.4 The fatigue tests results

The fatigue hysteresis loops under the frequency of 0.1 Hz frequency and the displacement amplitude of 10 mm are shown in Fig. 5. It is clearly observed that the extrusion force of the LED constantly reduces and gradually reaches to a stable state with the increase of the cycle number. The minimum value of the extrusion force amplitude is 145.8 kN, the decreasing rate is 13.11% comparing with the initial value 167.8 kN. The reason is that the yield strength is slightly reduced as the temperature increases. So the extrusion force will decrease slightly due to fatigue cycles, and tends to be stable in the end. During early fatigue tests, the energy of vibration absorbed by the LED can be converted into heat energy, which causes the increment of lead temperature. By continuing the tests the energy absorbed balances the energy released to the environment and the lead temperatures stop growing (Robinson and Greenbank 1976). Therefore, it can be predicted that the extrusion force of LED will not change easily no matter how the number of cycles increases. It can be concluded that the extrusion force and energy dissipation of the LED would decrease after fatigue tests, even if these reductions are not obvious.

3. Mathematical model and experimental verification

3.1 Mathematical model

Many researchers had been trying to find a suitable model to describe the mechanics characteristics of LED (Robinson and Greenbank 1976, Rodgers *et al.* 2006). The most typical model is the mathematical model proposed by Robinson, which considers the effect of velocity but ignores the effect of displacement amplitude. In addition, there are defects in the force-velocity loops when the extrusion force is negative. So a more accurate mathematical model needs to be proposed to accurately describe the performance of a LED. It can be seen from Figs. 3-4 that the force-velocity loop exhibits a nonlinear hysteretic characteristic and consists of two S-shaped branch curves. When the acceleration is greater than zero, the force-velocity loop is the lower branch curve. When the acceleration is less than zero, the force-velocity loop is the upper branch curve. When the acceleration closes to zero, the two curves almost overlap. The character of the single-branch force-velocity curve has a shape that recalls that of the hyperbolic tangent function. Therefore, the force-velocity loop can be constructed with a hyperbolic tangent function.

$$F = F_m \frac{e^{(v-\mathrm{sgn}(a))} - e^{-(v-\mathrm{sgn}(a))}}{e^{(v-\mathrm{sgn}(a))} + e^{-(v-\mathrm{sgn}(a))}}$$
(2)

where, F is the extrusion force; F_m is the maximum extrusion force of LED at the different loading conditions; v is the velocity of the bulged-shaft; a is the acceleration of the bulged-shaft and sgn is sign function. On that basis, the parameters k and s are introduced to Eq. (2), as follows

$$F = F_m \cdot \left(\frac{e^{k(v-s\cdot\mathrm{sgn}(a))} - e^{-k(v-s\cdot\mathrm{sgn}(a))}}{e^{k(v-s\cdot\mathrm{sgn}(a))} + e^{-k(v-s\cdot\mathrm{sgn}(a))}} \right)$$
(3)

where, k is the index parameter related with the slope of force-velocity hysteresis loop at the low velocity region; s is the parameter determined by experiment, which controls the width of

hysteresis region of the force-velocity loops.

3.2 Parameter identification

The experimental results under the frequency of 0.1 Hz frequency and the displacement amplitude of 10 mm are used to fit the parameters of the proposed mathematical model in this paper. Fig. 6 shows the relationship between the maximum extrusion force and velocity amplitude. The maximum extrusion force F_m increases less than the velocity amplitude according to a non-linear logarithmic relationship. Hence by increasing the velocity amplitude the extrusion force tends toward an asymptotic value and cannot increase indefinitely. Based on the above analysis, regression parameter is calculated by Eq. (4), as follows

$$F_m = a_1 + a_2 \ln(a_3 v) = a_1 + a_2 \ln(2a_3 \pi A f) \tag{4}$$

where, a_1, a_2 and a_3 are unknown coefficients determined from the experiment data; A is the displacement amplitude; f is the excitation frequency. The parameter F_m is identified by substituting the experimental data into Eq. (4). The results are $a_1 = 64$, $a_2 = 26$ and $a_3 = 8.11$. Fig. 6 shows the comparisons of parameters F_m between fitted values and identified values.

Fig. 7 shows a linear relationship between the parameter s and velocity amplitude. So the parameter s can be expressed as

$$s = b_1 + b_2 v = b_1 + b_2 (2\pi A f) \tag{5}$$

where, b_1 and b_2 are unknown coefficients determined from experimental data and the results are $b_1 = -0.526$ and $b_2 = 0.225$ respectively. Fig. 7 also shows the comparisons of parameters s between fitted values and identified values.

Fig. 8 shows the relationship between the parameter k and velocity amplitude. It can be seen that the index parameter k decreases with velocity amplitude increases, and shows a non-linear exponential relationship between them. Therefore, the parameter k can be expressed as
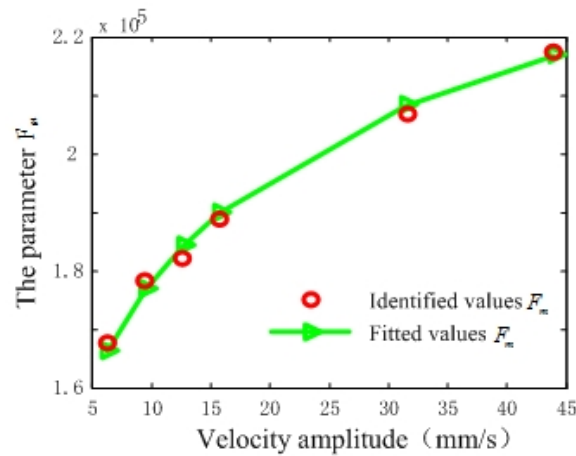

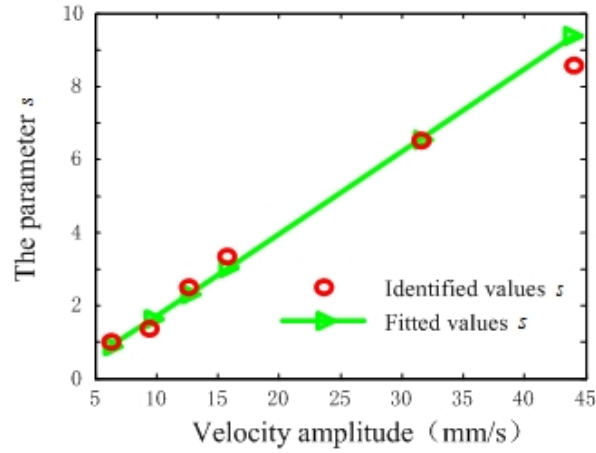Fig. 6 Comparisons of parameter F_m between fitted values and identified values

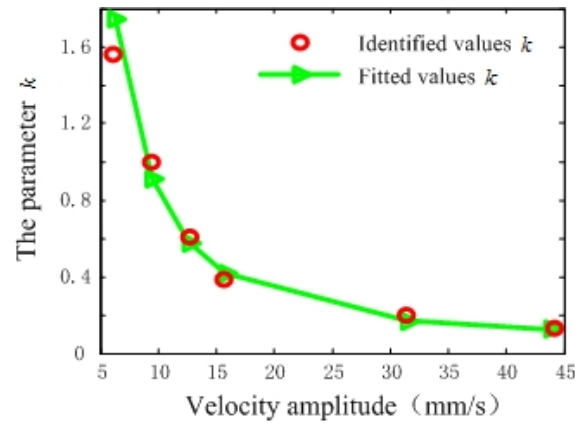Fig. 7 Comparisons of parameter *s* between fitted values and identified values

Fig. 8 Comparisons of parameter k between fitted values and identified values

$$k = c_1 + c_2 v^{c_3} = c_1 + c_2 (2\pi Af)^{c_3} \tag{6}$$

where, c_1, c_2 and c_3 are unknown coefficients which can be determined by experimental data. The parameter k is identified by substituting the experimental data into Eq. (6). The results are $c_1 = 0.06$, $c_2 = 38.7$ and $c_3 = -1.7$. Fig. 8 also shows the comparisons of parameters k between fitted values and identified values. From Figs. 6-8, we can see that the parameters are well fitted by using Eqs. (4)-(6).

3.3 Experimental verification

To demonstrate the accuracy of the proposed mathematical model for LED, the numerical results from the proposed mathematical model are compared with the experimental data which are not used for parameter identification. Fig. 9 shows the comparisons between the simulated curves
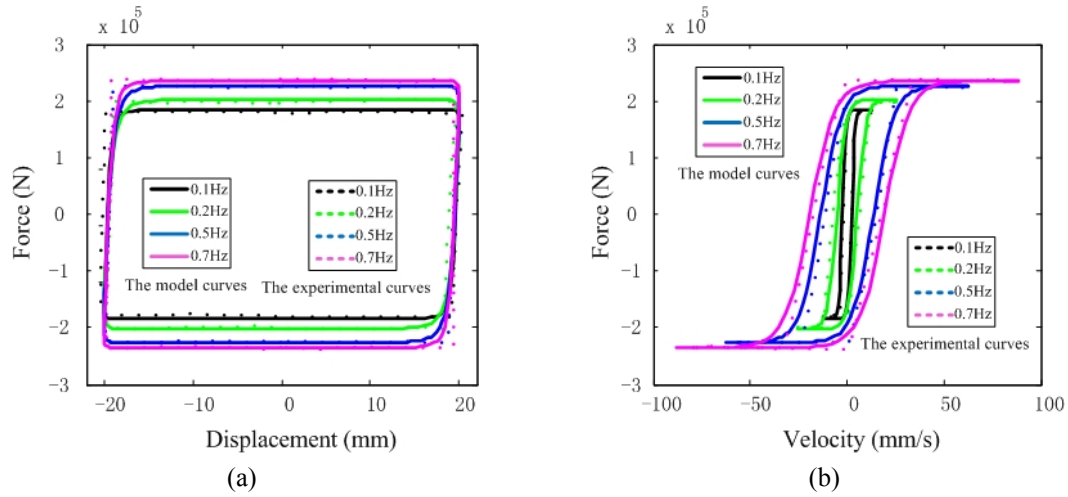
Fig. 9 Comparisons between the model curves and experimental curves under 20 mm
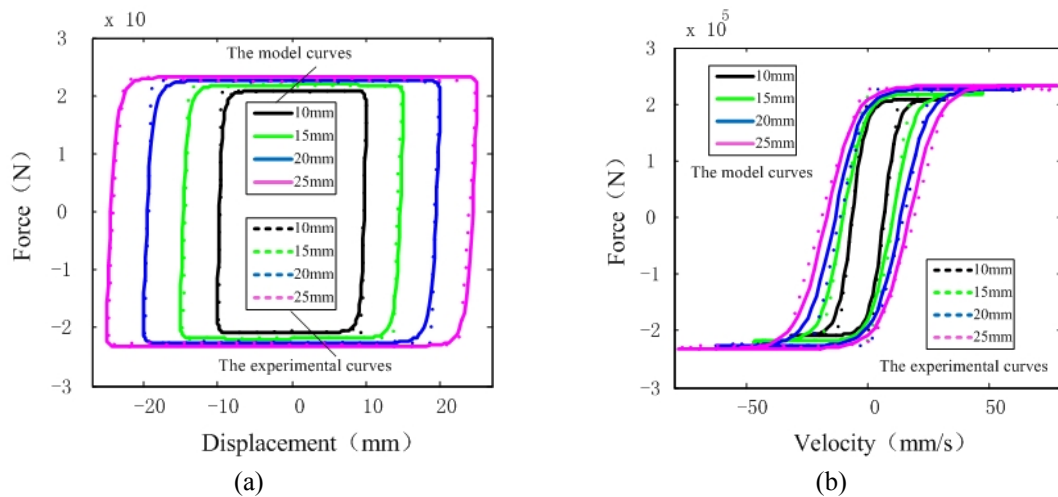displacement amplitude and various frequencies

Fig. 10 Comparisons between the model curves and experimental curves under 0.5 Hz frequency
and various displacement amplitudes

and the experimental curves under the displacement amplitude of 20 mm and various frequencies.

It can be seen that both the slope of the force-velocity loops in low velocity region and the width of the nonlinear hysteretic regions vary with excitation frequency. And the model curves have a quite good agreement with the experimental curves. The experimental data of the maximum extrusion force are 182.0 kN, 202.3 kN, 226.2 kN, and 237.8 kN under the frequencies of 0.1 Hz, 0.2 Hz, 0.5 Hz, and 0.7 Hz, the corresponding numerical results are 184.2 kN, 202.3 kN, 226.1 kN, and 234.8 kN, respectively. The maximum error is only 1.3%. From the perspective of energy dissipation, the results from the experiment test are shown in Table 4 at the displacement amplitude of 20 mm and various frequencies. Meanwhile, the energy by integrating the proposed

mathematical model curve under the frequencies of 0.1 Hz, 0.2 Hz, 0.5 Hz and 0.7 Hz are 14.36 kJ, 15.59 kJ, 17.42 kJ and 18.15 kJ, respectively. The maximum error between the experimental results and the proposed mathematical model results is 19.6%. The energy consumption of LED is significantly affected by displacement amplitude. There are differences in the displacement amplitude during testing, especially in the small displacement amplitude. But the proposed mathematical model result is accurate in this respect. Then, Fig. 10 shows the comparisons between the model curves and the experimental curves at the frequency of 0.5 Hz and various displacement amplitudes. It also can be seen that, in the low velocity region, the proposed mathematical model can simulate the characteristic of the extrusion force, as well as the width and the slope of the force-velocity loop.

Based on the above analysis, the results from the proposed mathematical model agree well with that of the experiment test in the maximum extrusion force and energy dissipation and can accurately reflect the relationship between the extrusion force, loading velocity (or excitation frequency) and displacement amplitude. In a word, the validity of the proposed mathematical model is confirmed from experimental results.

4. Earthquake mitigation effect of LEDs on large-span reticulated shell

4.1 Numerical model

To study the earthquake mitigation effect of LEDs on large-span reticulated shell structure and obtain the optimal arrangement positions of LEDs, 8 LEDs are installed in the Schwedler reticulated shell structure with three different forms, as shown in Fig. 11. In the first installation form is that the LEDs are installed between the two adjacent column joints, as shown in Fig. 11(a). In the second installation form is that the LEDs are installed between peripheral joints in the second row and column joints, as shown in Fig. 11(b). The last installation form is that the LEDs are installed in mixed mode, as shown in Fig. 11(c).

The overall geometric characteristics and sectional characteristics of the shell members are listed in Table 5.

The reticulated shell structure is braced with columns, the top of the columns is hinged on all the peripheral joints and the bottom is fixed on the ground, as shown in Fig. 11. The cross-section
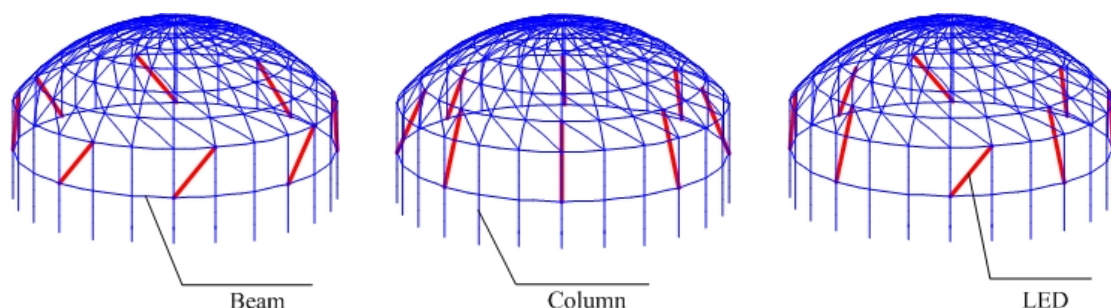
(a) The first installation form   (b) The second installation form   (c) The third installation form

Fig. 11 Arrangements of LEDs in Schwedler reticulated shell structure

Table 5 Schwedler reticulated shell parameters

Shell Span (m)	40	Radial main ribs (mm × mm)	Φ150 × 5
Shell height (m)	8	Circumferential Subsidiary ribs (mm × mm)	Φ120 × 5
Uniform loads (kN/m^2)	1	The remaining members (mm × mm)	Φ100 × 5

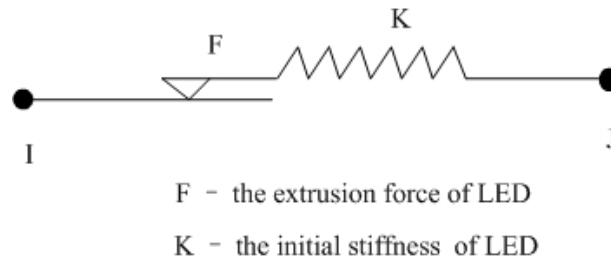F － the extrusion force of LED

K － the initial stiffness of LED

Fig. 12 Combin 40 element

size of the square column is set as 500 mm × 500 mm, and adjacent columns are connected by the beam, whose cross-section size is set as 300 mm × 600 mm. The strength grades of concrete are set as C40 for both column and beam. Steel strength grade of the member of Schwedler reticulated shell is set as Q235.

In order to obtain the earthquake mitigation effect of LEDs on the Schwedler reticulated shell structure, three-dimensional finite element models of the structure with and without LEDs are constructed by using the ANSYS software. While modeling, the member elements of the structure are simulated with Beam 188 element, and the LEDs are considered as a spring element in series with a frictional element and can be simulated with Combin 40 element in ANSYS, as shown in Fig. 12. Because the maximum extrusion force of the LED slightly increases with the increase of displacement amplitude, for convenience, the frictional force of the frictional element in Combin 40 element can be equivalent to 50 kN according to the finite element analysis results of the structure without LEDs. The stiffness K of the spring element in Combin 40 element can be calculated by the following equation as $K = F / x$, where F is the extrusion force, x is the displacement (2 mm), which can be obtained from test results. So, the initial stiffness K is set as 25000 kN/m. In addition, Taft and El Centro earthquake accelerograms with the peak value of 400 gal are selected as the earthquake excitations in simulations, and the durations for both Taft and El Centro earthquake accelerograms are 20 seconds.

4.2 Earthquake mitigation effect analysis

In order to verify earthquake mitigation effect of LEDs on large-span reticulated structure, displacement and acceleration responses of the Schwedler reticulated shell structure with and without LEDs are obtained by finite element analysis. Taking the vertex as reference point, the earthquake mitigation effects of the displacement and acceleration responses of the structure with LEDs can be calculated by Eq. (7).

$$e = \frac{\left|R_W\right|_{max} - \left|R_Y\right|_{max}}{\left|R_W\right|_{max}} \times 100\% \tag{7}$$

where, e is the percentage of the earthquake mitigation effect; R_Y is the responses of the structure with LEDs; R_W is the responses of the structure without LEDs.

The earthquake mitigation effects obtained from finite element analysis are listed in Table 6.

Taking El Centro earthquake accelerogram as an example, the vertex horizontal displacement and acceleration responses of the structure with LEDs are compared with that of the structure without LEDs, as shown in Figs. 13-15.

Fig. 13 shows the vertex displacement and acceleration responses comparisons between controlled and uncontrolled structure when the LEDs are installed in the first form. It can be seen that the maximum vertex displacement and acceleration responses of the structure without LEDs are 0.1522 m and 13.993 m/s², respectively. The maximum vertex displacement and acceleration responses of the structure with LEDs are 0.0881 m and 7.4802 m/s², respectively, which are reduced by 42.1% and 35.2%, respectively. Fig. 14 shows the vertex displacement and acceleration responses comparisons between controlled and uncontrolled structure when the LEDs are installed in the second form. The maximum vertex displacement and acceleration responses of the structure without LEDs are the same as before. The maximum vertex displacement and acceleration responses of the structure with LEDs are 0.0841 m and 7.4405 m/s², respectively, which are reduced by 44.8% and 36.2%, respectively. Fig. 15 shows the vertex displacement and acceleration responses comparisons between controlled and uncontrolled structure when the LEDs

Table 6 Earthquake mitigation effects of Schwedler reticulated shell with LEDs

Earthquake mitigation effects (%)		The first installation form	The second installation form	The third installation form
El Centro earthquake accelerogram	Vertex displacement	42.1	44.8	43.1
	Vertex acceleration	35.2	35.9	36.2
Taft earthquake accelerogram	Vertex displacement	62.9	63.8	64.5
	Vertex acceleration	48.9	49.2	48.4

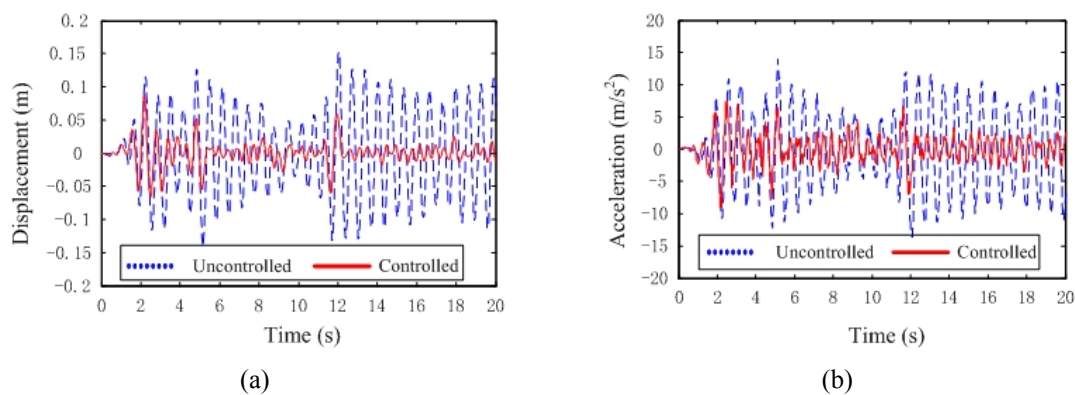(a)   (b)

Fig. 13 Vertex responses comparisons under the first installation form (El Centro earthquake accelerogram)
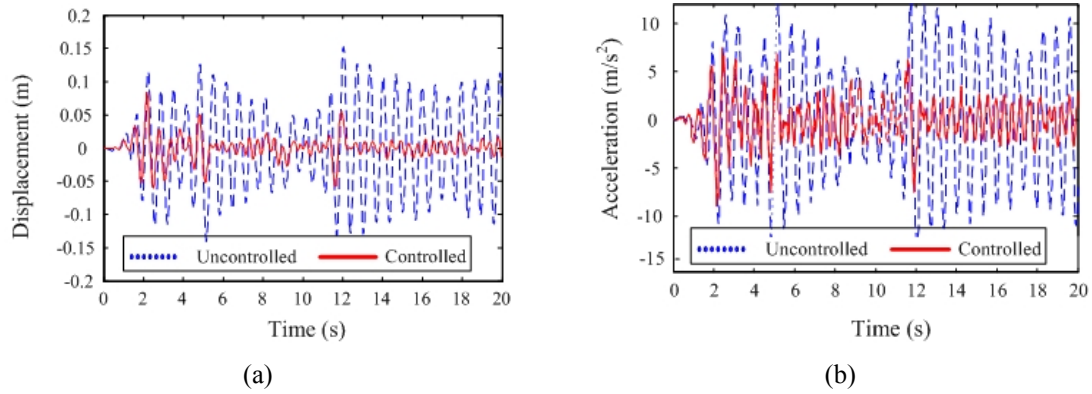
Fig. 14 Vertex responses comparisons under the second installation form (El Centro earthquake accelerogram)
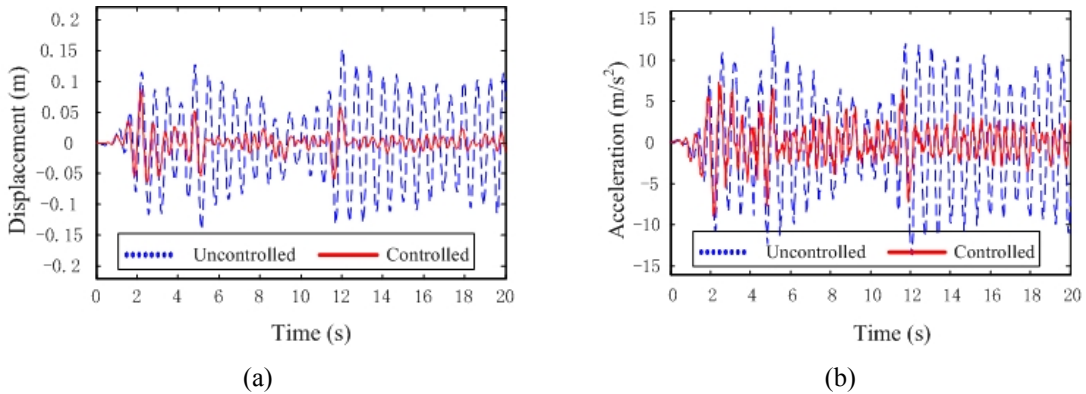

Fig. 15 Vertex responses comparisons under the third installation form (El Centro earthquake accelerogram)

are installed in the third form. The maximum vertex displacement and acceleration responses of the structure with LEDs are 0.0866 m and 7.373 m/s^2, respectively, which are reduced by 43.1% and 36.2%, respectively. Therefore, the second installation form of the LEDs is the optimal installation form for the reticulated shell structure. Meanwhile, the LED also plays an important role in the stability of Schwedler reticulated shell when the LEDs are installed between peripheral joints in the second row and column joints

Through above analysis, the displacement and acceleration responses of the structures with LEDs are reduced regardless of the damper is installed in what way. This is due to that the control forces produced by LEDs are equivalent to increasing stiffness and damping of structures: both are beneficial to decreasing displacement responses, and increasing of damping will decrease acceleration responses. Under different installation forms, the force-displacement hysteresis loops of the LED which occur the maximum relative displacement are shown in Fig. 16.

From Fig. 16, the maximum relative displacement between the shaft and cylinder of the damper are 0.0490 m, 0.0543 m, and 0.0459 m when the LEDs are installed in the first, second, and third forms. Compared with the first and third form, the relative displacement of the second form is increased by 10.8% and 18.3%, respectively. When the LEDs are installed in the second form,

(a) Hysteresis loops under the first installation form

(b) Hysteresis loops under the second installation form
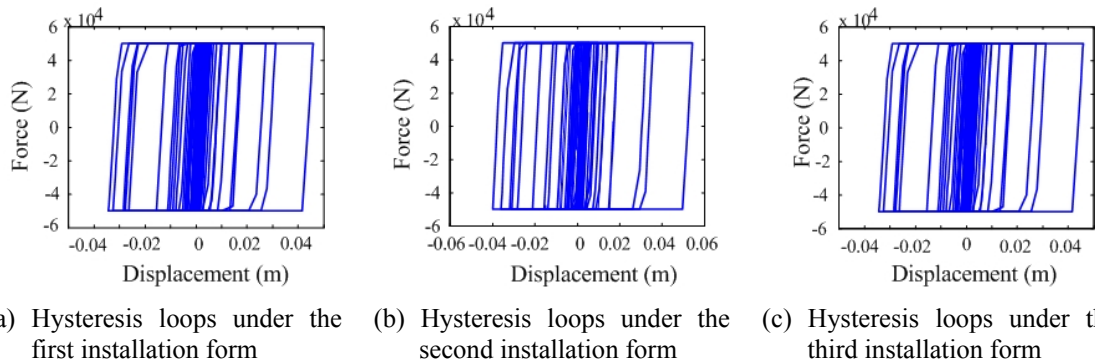
(c) Hysteresis loops under the third installation form

Fig. 16 Force-displacement hysteresis loops under different installation forms

the displacement and acceleration responses of the structures are smaller than the two other installation forms. At the same time, the maximum relative displacement is the largest when the LEDs are installed in the second form, which means that the seismic energy dissipated by LEDs is the largest.

5. Conclusions

In this paper, a full-scale Lead Extrusion Damper (LED) is presented. Through property tests and numerical analysis, the hysteretic characteristic of the extrusion force, energy dissipation capability, and fatigue properties of the LED are acquired. The mathematical model based on the experimental results is proposed and verified. Earthquake mitigation effects of the Schwedler reticulated shell with LEDs are analyzed. The following conclusions are obtained through experimental and numerical analysis.

- The maximum extrusion force increases with the increase of displacement amplitude and excitation frequency. The energy dissipation of LED is also increases with the displacement amplitude and excitation frequency.
- The extrusion force of LED can be neatly formulated from the parameters of the proposed mathematical model, and the results obtained by the mathematical model fit well with the results obtained by experimental tests.
- The displacement and acceleration responses of the Schwedler reticulated shell structures damped with suitable LEDs arrangements show a significant vibration mitigation in the behavior of such large-span structures.

References

Aida, T., Aso, T., Nakamoto, K. and Kawazoe, K. (1998), "Vibration control of shallow shell structures using a shell-type dynamic vibration absorber", *J. Sound Vib.*, **218**(2), 245-267.

Bel Hadj Ali, N. and Smith, I.F.C. (2010), "Dynamic behavior and vibration control of a tensegrity structure", *Int. J. Solids Struct.*, **47**(9), 1285-1296.

Bradley, B.A., Dhakal, R.P., Mander, J.B. and Li, L. (2008), "Experimental multi-level seismic performance assessment of 3D RC frame designed for damage avoidance", *Earthq. Eng. Struct. Dyn.*, **37**(1), 1-20.

Cousins, W.J. and Porritt, T.E. (1993), "Improvements to lead-extrusion damper technology", *Bulletin of the New Zealand National Society for Earthquake Engineering*, **26**(3), 342-348.

Garlock, M.M., Ricles, J.M. and Sause, R. (2005), "Experimental studies of full-scale posttensioned steel connections", *J. Struct. Eng.*, **131**(3), 438-448.

Housner, G.W., Bergman, L.A., Caughey, T.K., Chassiakos, A.G., Claus, R.O., Masri, S.F., Skelton, R.E., Soong, T.T., Spencer, B.F. and Yao, J.T.P. (1997), "Structural control: past, present and future", *J. Eng. Mech.*, *ASCE*, **123**(9), 897-971.

Kato, S., Kim, Y.B., Nakazawa, S. and Ohya, T. (2005), "Simulation of the cyclic behavior of J-shaped steel hysteresis devices and study on the efficiency for reducing earthquake responses of space structures", *J. Construct. Steel Res.*, **61**(10), 1457-1473.

Karolczuk, A. and Macha, E. (2005), "A review of critical plane orientations in multiaxial fatigue failure criteria of metallic materials", *Int. J. Fract.*, **134**(3), 267-304.

Manenti, S., Bontempi, F. and Malerba P.G. (2010), "A special kind of analysis: CFD modeling for design and assessment of bridge active control devices" *Proceedings of the Fifth International Conference on Bridge Maintenance*, *Safety*, *Management and Life-Cycle Optimization*, Philadelphia, PA, USA, July, CRC Press, Taylor & Francis Group, pp. 1436-1443.

Parulekar, Y.M., Reddy, G.R., Vaze, K.K. and Kushwaha, H.S. (2004), "Lead extrusion dampers for reducing seismic response of coolant channel assembly", *Nucl. Eng. Des.*, **227**(2), 175-183.

Robinson, W.H. and Greenbank, L.R. (1976), "Extrusion energy absorber suitable for the protection of structures during an earthquake", *Earthq. Eng. Struct. Dyn.*, **4**(3), 251-259.

Rodgers, G.W., Denmead, C., Leach, N., Chase, J.G. and Mander, J.B. (2006), "Experimental development and analysis of a high force/volume extrusion damper", *Proceedings of New Zealand Society for Earthquake Engineering Annual Conference*, Napier, New Zealand, March.

Rodgers, G.W., Mander, J.B., Chase, J.G., Dhakal, R.P., Leach, N.C. and Denmead, C.S. (2008), "Spectral analysis and design approach for high force-to-volume extrusion damper-based structural energy dissipation", *Earthq. Eng. Struct. Dyn.*, **37**(2), 207-223.

Towashiraporn, P., Park, J., Goodno, B.J. and Craig, J.I. (2002), "Passive control methods for seismic response modification", *Prog. Struct. Eng. Mater.*, **4**(1), 74-86.

Tsai, C.S., Lai, W.S., Chang, C.W. and Li, M.C. (2002), "Testing and analysis of a new Lead-extrusion damper American Society of Mechanical Engineers", *ASME 2002 Pressure Vessels and Piping Conference*, Vancouver, BC, Canada, August, pp. 215-220.

Wu, T. (2008), "A proposed methodology for strain-based failure criteria", *ASME 2008 Pressure Vessels and Piping Conference*, Chicago, IL, USA, July, Volume 7, pp. 631-637.

Xu, Z.D. (2009), "Horizontal shaking table tests on structures using innovative earthquake mitigation devices", *J. Sound Vib.*, **325**(1-2), 34-48.

Xu, Z.D., Shi, B.Q., Wu, K.Y. and Zeng, X. (2009a), "Vertical shaking table tests on the structure with viscoelastic multi-dimensional earthquake isolation and mitigation devices", *Science in China*, *Series E*: *Technological Sciences*, **52**(10), 2869-2876.

Xu, Z.D., Zeng, X., Wu, K.Y., Li, A.Q. and Xu, Q.Y. (2009b), "Horizontal shaking table tests and analysis on structures with multi-dimensional earthquake isolation and mitigation devices", *Science in China*, *Series E*: *Technological Sciences*, **52**(7), 2009-2016.

DL